THE JOURNAL OF BIOLOGICAL CHEMISTRY VOL. 289, NO. 49, pp. 33815–33825, December 5, 2014

An Alternative Mechanism for the Methylation of Phosphoethanolamine Catalyzed by *Plasmodium falciparum* Phosphoethanolamine Methyltransferase*◆

Received for publication, September 12, 2014, and in revised form, September 30, 2014 Published, JBC Papers in Press, October 6, 2014, DOI 10.1074/jbc.M114.611319

Suwipa Saen-oon[‡1], **Soon Goo Lee**[§1], **Joseph M. Jez**[§2], **and Victor Guallar**[‡¶3]

From the [‡]*Joint Barcelona Supercomputing Center-Centre for Genomic Regulation-Institute for Research in Biomedicine Research Program, Carrer de Jordi Girona 29, 08034 Barcelona, Spain, the* [§]*Department of Biology, Washington University, St. Louis, Missouri 63130, and the* [¶]*Catalan Institution for Research and Advanced Studies, Barcelona 08010, Spain*

Background: In *Plasmodium*, phosphoethanolamine methyltransferase (PfPMT) is essential for normal growth and development.
Results: Computational, biochemical, and structural studies suggest catalytic and structural roles for Asp-128 in PfPMT.
Conclusion: Asp-128 is critical for specific methylation of phosphoethanolamine and not other phosphobases.
Significance: This work provides new insight on the evolution of multiple substrate activity in PMT from different organisms.

The phosphobase methylation pathway catalyzed by the phosphoethanolamine methyltransferase in *Plasmodium falciparum* (PfPMT), the malaria parasite, offers an attractive target for antiparasitic drug development. PfPMT methylates phosphoethanolamine (pEA) to phosphocholine for use in membrane biogenesis. Quantum mechanics and molecular mechanics (QM/MM) calculations tested the proposed reaction mechanism for methylation of pEA involving the previously identified Tyr-19–His-132 dyad, which indicated an energetically unfavorable mechanism. Instead, the QM/MM calculations suggested an alternative mechanism involving Asp-128. The reaction coordinate involves the stepwise transfer of a proton to Asp-128 via a bridging water molecule followed by a typical S_n2-type methyl transfer from *S*-adenosylmethionine to pEA. Functional analysis of the D128A, D128E, D128Q, and D128N PfPMT mutants shows a loss of activity with pEA but not with the final substrate of the methylation pathway. X-ray crystal structures of the PfPMT-D128A mutant in complex with *S*-adenosylhomocysteine and either pEA or phosphocholine reveal how mutation of Asp-128 disrupts a hydrogen bond network in the active site. The combined QM/MM, biochemical, and structural studies identify a key role for Asp-128 in the initial step of the phosphobase methylation pathway in *Plasmodium* and provide molecular insight on the evolution of multiple activities in the active site of the PMT.

Methyltransferases are ubiquitous in biochemical and cellular processes (1). Using *S*-adenosylmethionine (AdoMet)[4] as the methyl donor, this diverse group of enzymes catalyzes the modification of macromolecules and metabolites using a range of chemical strategies, including proximity, desolvation effects, acid-base catalysis, and metal-dependent deprotonation (1–3). The action of these enzymes is crucial for metabolic function, controlling gene regulation, and is linked to assorted diseases (3). Recent studies also suggest an important role for methyltransferases in plants, nematodes, and the apicomplexan parasite *Plasmodium falciparum* in the synthesis of phospholipid precursors (4–6).

In plants, nematodes, and *Plasmodium*, the phosphobase methylation pathway is used for the synthesis of phosphocholine (pCho) for phosphatidylcholine production (Fig. 1, *top*). The methylations that convert phosphoethanolamine (pEA) to phosphomonomethylethanolamine (pMME), phosphodimethylethanolamine (pDME), and pCho are performed by phosphoethanolamine methyltransferases (PMT). Three types of PMT with varied domain architectures are found in different organisms (6). Plant PMT are di-domain enzymes (~450 amino acids) with one active site (PMT1) catalyzing the methylation of pEA to pMME, and a second active site (PMT2) that catalyzes the conversion of pMME to pDME and pDME to pCho (7). In nematodes, two PMT retain the di-domain organization (~430–480 amino acids) of the plant enzyme, except one of the domains in each nematode PMT is vestigial (8–11). This leads to distinct PMT1 and PMT2 enzymes in *Caenorhabditis elegans* and other nematodes. Unlike plants and nematodes, *P. falciparum* contains a single domain PMT (PfPMT; 266 amino acids) that catalyzes all three methylation steps in the phosphobase pathway

* This work was supported, in whole or in part, by National Institutes of Health Grant AI-097119 (to the Jez laboratory). This work was also supported by funds from the Barcelona Supercomputer Center and the Spanish Ministry of Education and Science through Project CTQ2013-48287 (to the Guallar laboratory). Portions of this work were carried out at the Argonne National Laboratory Structural Biology Center of the Advanced Photon Source, a national user facility operated by the University of Chicago for the Department of Energy Office of Biological and Environmental Research and supported by Contract DE-AC02-06CH11357.
◆ This article was selected as a Paper of the Week.
The atomic coordinates and structure factors (codes 4R6W and 4R6X) have been deposited in the Protein Data Bank (http://wwpdb.org/).
[1] Both authors contributed equally to this work.
[2] To whom correspondence may be addressed. E-mail: jjez@biology2.wustl.edu.
[3] To whom correspondence may be addressed. E-mail: victor.guallar@bsc.es.

[4] The abbreviations used are: AdoMet, to *S*-adenosylmethionine; AdoHcy, adenosylhomocysteine; PfPMT, *P. falciparum* phosphoethanolamine methyltransferase; pEA, phosphoethanolamine; pCho, phosphocholine; QM/MM, quantum mechanics and molecular mechanics; pMME, phosphomonomethylethanolamine; pDME, phosphodimethylethanolamine; PMT, phosphoethanolamine methyltransferase; PDB, Protein Data Bank; ITC, isothermal titration calorimetry; MD, molecular dynamics; r.m.s.d., root mean square deviation.

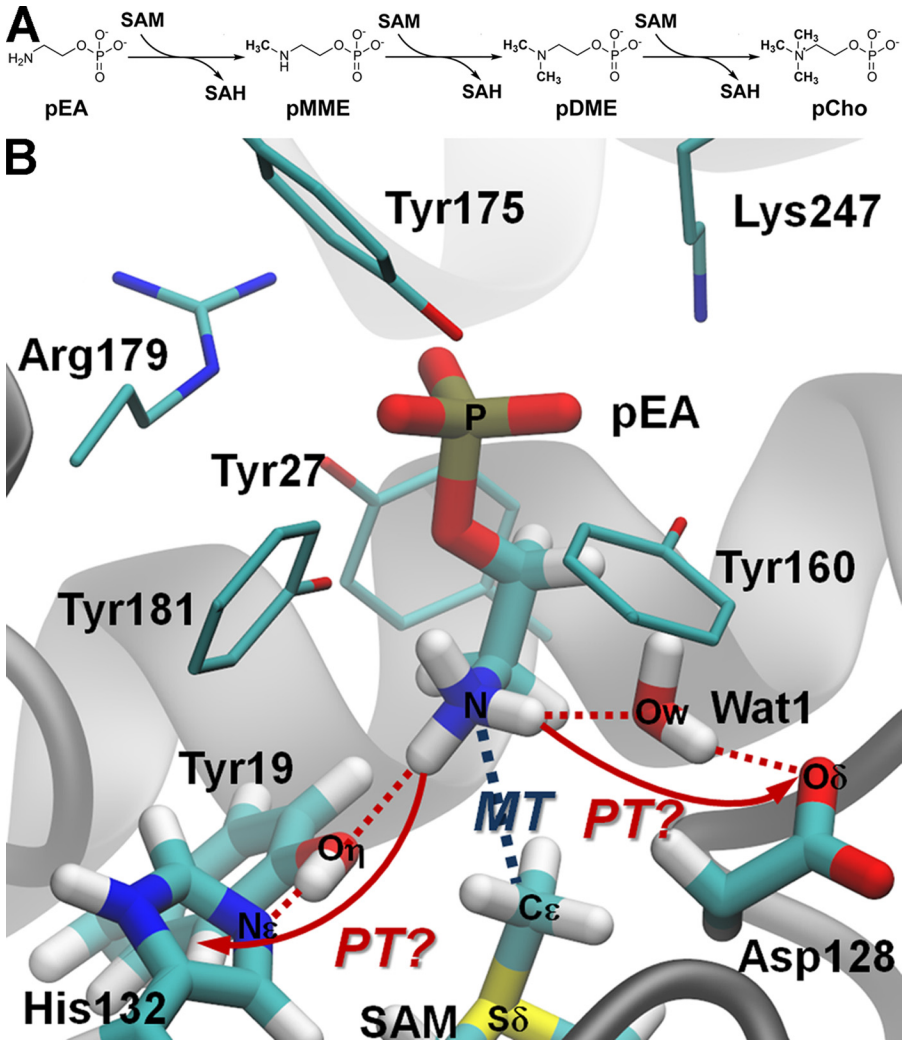

FIGURE 1. **Phosphobase methylation pathway and the active site of the PfPMT.** *Top,* phosphobase methylation pathway of *P. falciparum* showing the sequential methylation of pEA to pMME, pDME, and pCho. *B,* active site structure illustrating two possible pathways for deprotonating pEA. The *red dotted lines* indicate the alternative proton transfer (*PT*) routes through either the Tyr-19–His-132 dyad or the water-mediated interaction with Asp-128. The methyl transfer (*MT, blue dotted line*) step from AdoMet to pEA is also shown. *SAM* is AdoMet.

(12). PfPMT plays an important role in the metabolism of the malaria parasite by supporting the synthesis of phospholipids during reproduction and growth. Disruption of the PfPMT gene leads to a reduced phosphatidylcholine synthesis from serine, growth and survival defects, and the loss of parasite transmission to mosquitoes (12–14). Because of its critical role in *Plasmodium* and the lack of PMT homologs in mammals, PfPMT, along with other enzymes in phospholipid metabolism, is a target for antiparasitic drug development (5, 6, 15–17).

X-ray crystal structures of PfPMT in complex with various substrates and inhibitors and extensive biochemical characterization provide insight on the organization of the AdoMet and phosphobase-binding sites in the enzyme (Fig. 1, *bottom*) (18, 19). In particular, electrostatic interactions provided by Arg-179 and Lys-247, together with hydrogen bond interactions contributed by hydroxyl groups of several tyrosine residues, are critical for phosphobase binding. In addition, Tyr-19 and His-132, which are positioned between AdoMet and phosphobase-binding sites, were suggested as catalytic residues (18). In the proposed reaction mechanism (Fig. 1, *bottom*), His-132 functions as a general base to abstract a proton from the hydroxyl group of Tyr-19. Next, the negatively charged tyrosine oxygen interacts with a hydrogen atom on the substrate amine, orienting the lone pair of electrons toward the methyl group of AdoMet to facilitate the bimolecular nucleophilic substitution (S_n2) methyl transfer to pEA.

In this study, we combine computational modeling with protein crystallography and site-directed mutagenesis to re-examine the methylation of pEA catalyzed by PfPMT. Initially, we tested the ability of the proposed catalytic Tyr-19–His-132 dyad in deprotonating pEA, which suggests an energetically unfavorable mechanism. Instead, the quantum mechanical/molecular mechanical (QM/MM) calculations suggest an alternative mechanism involving Asp-128 to deprotonate pEA via a bridging water molecule (Fig. 1, *bottom*). Biochemical analysis of site-directed mutants targeting Asp-128 shows a loss of activity with pEA as a substrate but retains activity with pDME. The x-ray crystal structures of the PfPMT·D128A mutant in complex with *S*-adenosylhomocysteine (AdoHcy) and either pEA or pCho reveal structural changes in the active site. Over-

TABLE 1

Calculated pK_a values of the amine group of pEA

Different starting conformations obtained from the x-ray crystal structure of PfPMT (PDB code 3UJ7 (18)) and snapshots of molecular dynamic simulations were used for pK_a calculations in PROPKA version 3.1.

Model	PfPMT·pEA	PfPMT·pEA·AdoMet
X-ray structure	12.37	9.12
M1	8.36	8.06
M2	11.04	9.44
M3	10.31	8.42
M4	11.50	8.34
Average	10.72 ± 1.51	8.68 ± 0.52

all, these studies suggest the importance of Asp-128 in the initial step of the phosphobase methylation pathway catalyzed by PfPMT and provide insight on the evolution of multiple activities in the active site of the PMT from the malaria parasite.

EXPERIMENTAL PROCEDURES

Computational Model Setup—The initial structure of PfPMT·pEA·AdoMet ternary complex was modeled from the crystal structure of PfPMT in complex with pEA and AdoHcy (18; PDB code 3UJB). AdoHcy was amended to AdoMet by adding one methyl group on Sγ based on the geometric parameters of AdoMet bound to PfPMT (PDB code 3UJ7 (18)). The system was prepared using Protein Wizard (20) within the Schrodinger suite to optimize hydrogen-bonded networks and assign proper protonation states for ionizable residues at pH 7. In particular, all histidines were singly protonated (neutral) with His-82 and His-218 having the proton at their Nϵ with all other histidines protonated at the Nδ. The system was then equilibrated with 1 ns of molecular dynamics (MD) in a water box using weak harmonic constraints (5 kcal mol^{-1} $Å^2$) for all heavy atoms to maintain their active site configuration.

The protonation state of the amine group in pEA was estimated using PROPKA (21). Five different PfPMT·pEA·AdoMet conformations, including the crystal structure and four MD snapshots along the equilibration, were used and resulted in an estimated pK_a of 10.72 ± 1.51 (Table 1). Addition of AdoMet to the active site model decreases the pK_a to 8.68 ± 0.52 because of electrostatic interaction with the positive charge of the AdoMet methyl group. A similar pK_a shift (from ~11 to ~8) in the presence of the AdoMet cofactor was reported for lysine methyltransferase (22). Thus, we assigned the pEA substrate in its protonated form as NH_3^+-pEA.

QM/MM Reaction Profiles—All QM/MM calculations were carried out using the QSite program of the Schrodinger Suite (QSite, version 5.7; Schrödinger, LLC: New York). The QM part was treated at the M06/6-31G(d,p) level of theory (23), and the MM part was described with the OPLS force field (24). The hydrogen link atom approach was used for the QM/MM boundary treatment. During the QM/MM geometry optimization, the QM region and all MM atoms within a distance of 10 Å from any atom in NH_3^+-pEA and AdoMet were allowed to relax. To calculate the QM/MM reaction profiles, we performed a linear scanning approach by imposing distance constraints. For each reaction profile, we carried out three iterative scans driving the reaction coordinate forward, backward, and repeatedly forward between reactant and product states. Analytical harmonic second derivatives were calculated to confirm the nature of the stationary point, with no imaginary eigenvalues for minima and only one imaginary eigenvalue for transition states.

Molecular Dynamics Simulations—All MD simulations were carried out with AMBER11.0 using the AMBER03 (25) and general AMBER (GAFF) (26) force field for protein and substrates, respectively. Atomic charges on pEA and AdoMet were determined at the HF/6–31G(d) level of theory using the restrained electrostatic potential approach (27). The long range electrostatic interaction was treated with particle mesh Ewald (28), and the short range cut off for nonbonded interactions was set to 12 Å. The PfPMT·pEA·AdoMet system was immersed in a cubic box of TIP3P water molecules extending 15 Å from solute atoms in all three dimensions. The system was initially relaxed by imposing a position constraint on the heavy atoms of the PfPMT·pEA·AdoMet complex over 5,000 cycles of minimization procedure. The constraint was gradually released while heating the system in the NVT ensemble from 10 to 300 K over 50 ps. Temperature was controlled by the Andersen temperature coupling scheme, and the pressure was controlled by the isotropic position scaling protocol applied in AMBER. The SHAKE algorithm was employed to constrain all hydrogen atoms, and the time step was set to 2.0 fs (29). The simulation was equilibrated for 1 ns, prior to MD runs of 10 ns at a target temperature of 300 K and pressure of 1 atmosphere. Three independent MD simulations were run. In all simulations, the root-mean-square deviation (r.m.s.d.) of the enzyme backbone from their positions in the crystal structure was less than 1.2 Å. Structural and water-shell analyses from MD trajectories were carried out with PTRAJ module (30).

pEA binding affinities were estimated using the MM/GBSA approach (31). The enthalpy term was computed from 1,000 snapshots evenly extracted from a single MD trajectory. Because of the high computational demand for the normal mode analysis, we used only 10 snapshots for each ternary complex to estimate the contribution of the entropy to binding (extracting structures every 1 ns).

Site-directed Mutagenesis, Protein Expression, and Protein Purification—Generation of PfPMT D128A, D128E, D128Q, and D128N mutants used the QuikChange PCR mutagenesis method with the pET28a-PfPMT vector (18) as a template. Wild-type and mutant PfPMT were expressed in *Escherichia coli* BL21(DE3) and purified by nickel-affinity and size-exclusion chromatographies, as described previously (18).

Enzyme Assays and Isothermal Titration Calorimetry—Standard assay conditions for PMT activity were 0.1 M Hepes-KOH (pH 8), 2 mM Na_2EDTA, 10% glycerol, 2.5 mM AdoMet (100 nCi of [*methyl*-^{14}C]AdoMet), and 5 mM phosphobase substrate (either pEA or pDME) in 100 μl. Protein (10 μg) was incubated for 10 min at room temperature with reactions terminated and product quantified as described previously (8, 9). Steady-state kinetic analysis of wild-type and mutant PfPMT was performed as described previously (8, 9, 18). Isothermal titration calorimetry (ITC) was used to monitor AdoHcy and pCho binding to wild-type and mutant PfPMT, as described previously (10, 18).

Protein Crystallography—Crystals of the PfPMT-D128A·AdoHcy·pEA and PfPMT-D128A·AdoHcy·pCho complexes were grown by the vapor diffusion method in hanging drops of a 1:1 mixture of protein (13.5 mg/ml) and crystallization buffer

TABLE 2
Crystallographic statistics

	PfPMT-D128A·AdoHcy·pCho	PfPMT-D128A·AdoHcy·pEA
Crystal		
Space group	P2	P2
Cell dimensions	a = 77.17 Å, b = 44.06 Å, c = 89.15 Å; β = 108.1°	a = 76.83 Å, b = 43.65 Å, c = 88.05 Å; β = 107.8°
Data collection		
Wavelength (Å)	0.979	0.979
Resolution range (Å) (highest shell resolution)	30.4–1.59 (1.62–1.59)	38.7–2.60 (2.64–2.60)
Reflections (total/unique)	270,106/76,333	57,984/17,579
Completeness (highest shell)	99.6% (99.6%)	99.4% (99.3%)
$\langle I/\sigma \rangle$ (highest shell)	22.5 (2.2)	9.1 (1.9)
R_{sym}[a] (highest shell)	7.9% (52.1%)	16.5% (62.7%)
Model and refinement		
R_{cryst}[b]/R_{free}[c]	15.9%/18.8%	20.3%/25.8%
No. of protein atoms	4,310	4,242
No. of water molecules	715	143
No. of ligand atoms	74	68
r.m.s.d., bond lengths (Å)	0.007	0.002
r.m.s.d., bond angles (°)	1.026	0.585
Average B-factor (Å^2)-protein, water, ligand	22.2, 36.8, 18.4	27.4, 28.7, 25.7
Stereochemistry: most favored, allowed, outliers	99.0, 1.0, 0%	97.9, 2.1, 0%

[a] $R_{sym} = \Sigma|I_h - \langle I_h \rangle|\Sigma I_h$, where $\langle I_h \rangle$ is the average intensity over symmetry.
[b] $R_{cryst} = \Sigma||F_o| - |F_c||/\Sigma|F_o|$, where summation is over the data used for refinement.
[c] R_{free} is defined the same as R_{cryst} but was calculated using 5% of data excluded from refinement.

(20% PEG-8000, 0.1 M sodium cacodylate (pH 6.5), 0.2 M sodium acetate, 20 mM tris(2-carboxyethyl)phosphine, 5 mM AdoHcy, and 5 mM pEA/pCho). Diffraction data were collected at beamline 19-ID of the Argonne National Lab Advanced Photon Source. HKL3000 (32) was used for indexing, integration, and scaling of diffraction data. The crystal structure of each complex was determined by a molecular replacement using PHASER (33) and the PfPMT·AdoMet·PO_4^{2} structure (PDB code 3UJ7 18) with ligands removed and Asp-128 mutated to an alanine as the search model. Model building and refinement were performed in COOT (34) and PHENIX (35), respectively. Data collection and refinement statistics are summarized in Table 2. Coordinates and structure factors for the PfPMT-D128A·AdoHcy·pEA (PDB code 4R6W) and PfPMT-D128A·AdoHcy·pCho (PDB code 4R6X) complexes have been deposited in the Protein Data Bank.

RESULTS

Modeling of Phosphoethanolamine Methylation Catalyzed by PfPMT—Starting from the crystal structure of PfPMT·pEA·AdoMet complex after a 1-ns equilibration, we examined the previously proposed mechanism in which Tyr-19 and His-132 deprotonate pEA (18). The QM region included pEA, Tyr-19, His-132, and part of AdoMet (excluding the adenine base) for a total of 76 atoms. We performed QM/MM scanning where the reaction coordinate was defined as the distance between the Nϵ of His-132 and the hydroxyl hydrogen of Tyr-19. In doing so, a proton was pulled from Tyr-19 to His-132 starting from a distance of 1.8 Å (at the reactant) to 1.0 Å (at the product). The proton transfer reaction profile displayed a 21 kcal/mol endothermic profile, with energy increasing monotonically and no energy minimum corresponding to products/intermediates (Fig. 2*A*). Upon the approach of a proton from Tyr-19 to His-132, simultaneous proton transfer from NH_3^+-pEA to a negatively charged (deprotonated) Tyr-19 did not take place. Moreover, the forced product of this proton transfer path (Tyr-19$^-$–His-132$^+$) reverts to the tyrosine when removing the constraint on the reaction coordinate.

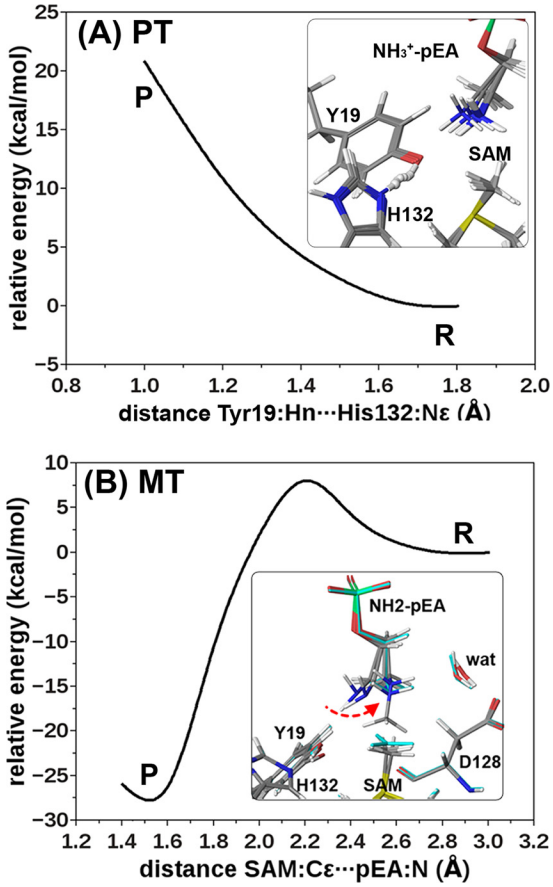

FIGURE 2. **QM/MM energy profiles for proton transfer and methyl transfer reactions.** *A*, endothermic energy profile for the proton transfer involving Tyr-19 and His-132. *B*, energy profile for a direct methyl transfer (*MT*) from AdoMet to neutral NH_2-pEA. *Insets* depict the processes. In particular, in *B* we *highlight* the rotation of the amine group, movement of the water molecule, and the S_n2 linear in-line transition state (*cyan color*). *SAM* is AdoMet.

Based on this lack of deprotonation from the Tyr-His dyad, we manually took a proton from pEA and performed a methyl transfer linear scanning, aiming to observe an enhanced structure for proton abstraction. Thus, we perturbed the distance

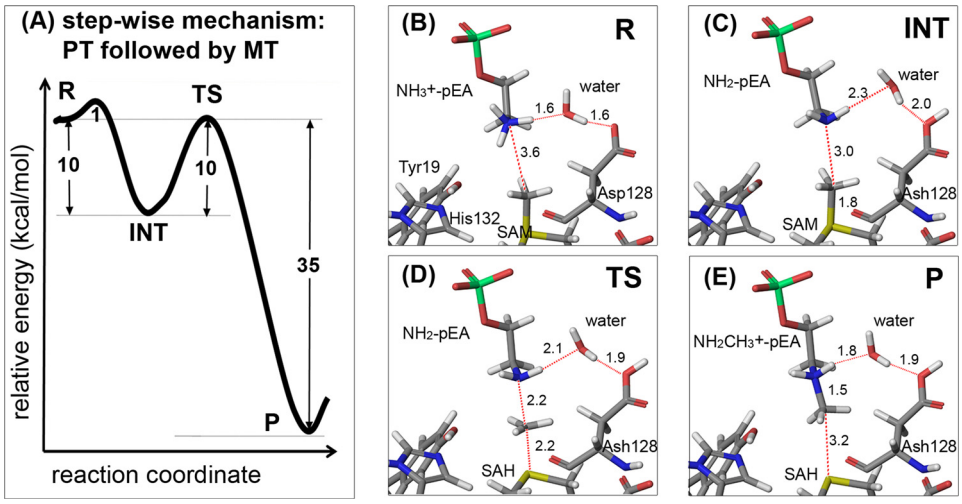

FIGURE 3. **Potential role of Asp-128 in methylation of phosphoethanolamine.** *A*, QM/MM reaction energy profile (kcal/mol) for the stepwise path describing the proton transfer (*PT*) from NH_3^+-pEA to Asp-128 via a water molecule, and the methyl transfer (*MT*) from AdoMet to NH_2-pEA. *B–E*, structures along the reaction coordinate of the stepwise mechanism are shown as follows for *B–E*: reactant (*R*), intermediate (*INT*), transition state (*TS*), and product (*P*).

between the methyl group of AdoMet (Cϵ atom) and the amine nitrogen in neutral NH_2-pEA, using the same QM region defined above. Along the methyl transfer, no significant improvement (indication) of proton transfer between pEA and Tyr-19 was observed. Interestingly, there was a rotation of the substrate amine group, which positioned the substrate lone pair for an S_n2-type reaction and enhanced its interaction with a crystallographically determined water molecule, Wat (Fig. 2*B*). This conformational rearrangement allows for hydrogen bond interactions between pEA and Wat1 (2.5 Å N–O distance) and between Wat1 and Asp-128 (2.6 Å O–O distance). These distances were obtained after a QM/MM minimization, and inclusion of missing vibrational (temperature and zero point) energies would increase these distances to ~2.7 Å. In this orientation, although Asp-128 is located almost 6 Å away from the amine group of pEA, a hydrogen bond network via a water bridge may contribute to catalysis. The same conformational rearrangement results were obtained when repeating the QM/MM calculations by extending the QM region to include Wat and Asp-128, for a total of 96 atoms.

Potential Role of Asp-128 in the Methylation of Phosphoethanolamine—From the QM/MM results described above, an alternative mechanism where Asp-128 acts as a general base to deprotonate pEA through a water bridge is possible. In this reaction mechanism, Asp-128 activates the water molecule to abstract a proton from NH_3^+-pEA, followed by transfer of the methyl group from AdoMet to neutral NH_2-pEA, which leads to formation of pMME and AdoHcy. To test this hypothesis, the proton and methyl transfer reaction profiles via stepwise and concerted mechanisms, using the largest (96 atoms) quantum region, were explored.

The reaction profile for a stepwise mechanism involving Asp-128 is presented in Fig. 3*A*. The first proton transfer step from NH_3^+-pEA to Asp-128 via the water proceeds easily (activation energy ~1 kcal/mol) to form a more stable neutral intermediate (NH_2-pEA·Asp-128·AdoMet, with Ash referring to a protonated Asp) with 10.3 kcal/mol lower energy than the reactant state (R; NH_3^+-pEA·Asp-128·AdoMet). The following

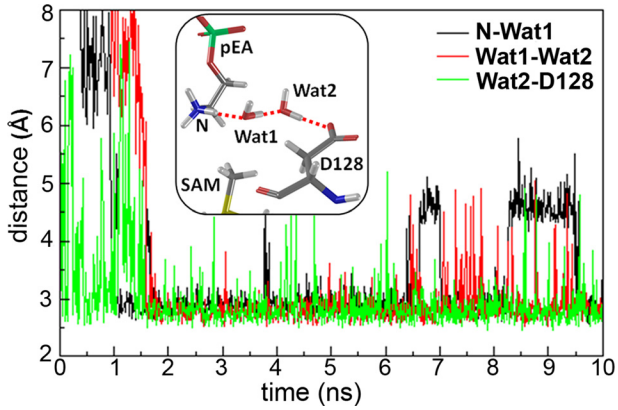

FIGURE 4. **Stability of the water network in MD simulations.** Plot of heteroatom distances between water molecules connecting pEA to Asp-128 throughout MD simulations. The *inset* presents a representative snapshot showing two water molecules forming the pEA–Asp-128 bridge. *SAM* is AdoMet.

methyl transfer step undergoes a typical S_n2 process with an energy barrier of 10.0 kcal/mol to produce a highly stable product ($NH_2CH_3^+$-pEA·Ash-128·AdoHcy). The overall reaction is exothermic by 35.3 kcal/mol. The structures of the reaction sequence (Fig. 3, *B–E*) suggest that the intermediate presents S_n2-ready spatial ordering, where the amine lone pair electrons point directly to the methyl carbon of AdoMet. In this orientation, the distance between them is about 3.0 Å, and the angle is ~171°. The methyl transfer transition state has an imaginary frequency of $-424i$ cm^{-1}, exhibits a linear AdoMet:Sδ···AdoMet:Cϵ···pEA:N configuration with an angle of 173°, and is almost equidistant between bond breaking (2.18 Å) and forming (2.20 Å). All attempts to produce a concerted proton transfer/methyl transfer pathway dramatically increased the energy barriers to ~70 kcal/mol.

Water Network Stability and the Methylation of Phosphoethanolamine—To probe the presence of the water network connecting pEA and Asp-128, three 10-ns MD runs were performed. In each simulation, the stability of the water network was observed (Fig. 4), although several water exchanges with bulk solvent were observed. Moreover, in 70% of the simulations, the network consists of two water molecules (*inset* of Fig.

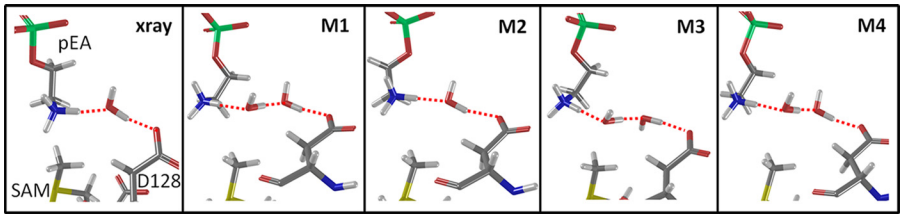

FIGURE 5. **Starting configurations for MD simulations.** Different starting configurations obtained from MD trajectories for QM/MM calculations showing the hydrogen bond network between pEA and Asp-128 through the water bridge. *SAM* is AdoMet.

TABLE 3

Summary of activation energy (*EA*#) and reaction energy (Δ*E*) for the proton transfer step from QM/MM calculations using different starting configurations

Structural parameters of the reactant state are reported on the full QM/MM optimization at M06/6-31G(d,p) level of theory.

	Crystal	M1	M2	M3	M4
No. of waters in bridge	1	2	1	2	2
EA# (kcal/mol)	1.0	4.0	4.4	5.1	6.0
Δ*E* (kcal/mol)	−10.3	−3.4	−2.6	−1.8	1.70
Reactant parameters					
AdoMet:Sδ···AdoMet:Cϵ (Å)	1.81	1.80	1.81	1.81	1.81
AdoMet:Cϵ···pEA:N (Å)	3.57	3.74	3.66	4.13	3.97
∠ Sδ-Cϵ-N (°)	165	141	147	144	134
pEA:N···Wat1:Ow (Å)	2.64	2.68	2.72	2.70	2.71
Wat1:Ow···Wat2:Ow (Å)		2.63		2.63	2.64
Wat2:Ow···Asp-128:Oδ (Å)	2.60	2.63	2.80	2.71	2.71

TABLE 4

Summary of activation energy (*EA*#) and reaction energy (Δ*E*) for methyl transfer step from QM/MM calculations using different starting configurations

Geometrical parameters for the methyl transfer in the reactant, transition state, and product state of different initial configurations.

	Crystal	M1	M2	M3	M4	Average
EA# (kcal/mol)	10.0	7.1	9.4	14.8	7.3	9.7 ± 3.2
Δ*E* (kcal/mol)	−25.0	−31.8	−34.4	−27.0	−31.7	−30.0 ± 3.9
Reactant						
*d*1 (Å)[a]	3.00	2.89	2.97	3.14	2.91	2.98 ± 0.10
*d*2 (Å)[b]	1.83	1.82	1.83	1.82	1.83	1.83 ± 0.01
θ (°)[c]	171	151	160	136	163	156 ± 13
Transition state						
*d*1 (Å)	2.20	2.20	2.24	2.20	2.25	2.22 ± 0.02
*d*2 (Å)	2.18	2.17	2.27	2.28	2.27	2.23 ± 0.05
θ (°)	173	170	164	169	176	170 ± 4
Product						
*d*1 (Å)	1.49	1.48	1.49	1.49	1.49	1.4 9 ± 0.00
*d*2 (Å)	3.28	3.14	3.75	3.62	3.32	3.42 ± 0.25
θ (°)	160	163	130	126	173	150 ± 21

[a] *d*1 is the forming bond distance between AdoMet:Cϵ···pEA:N in Å.
[b] *d*2 is the breaking bond distance between AdoMet:Sδ···AdoMet:Cϵ in Å.
[c] *θ* is the AdoMet:Sδ···AdoMet:Cϵ···pEA:N angle in degrees.

4). Despite the presence of two waters, the QM/MM results indicate that the proton transfer to Asp-128 is associated with low energy barriers. Four additional QM/MM energy profiles were obtained from different MD snapshots (Fig. 5), with three simulations (M1, M3, and M4) presenting a two water network between substrate and Asp-128. The average barrier for proton transfer and methyl transfer steps were 4.1 ± 1.9 and 9.7. ± 3.2 kcal/mol, respectively, and are in good agreement with the simulation based on the x-ray crystal structure. Importantly, even with a two water bridge, all of the proton transfer reactions from NH_3^+-pEA to Asp-128 undergo a concerted asynchronous mechanism with low energy barriers (4–6 kcal/mol; Table 3). The subsequent methyl transfers proceed through a mechanism consistent with an S_n2 reaction (Table 4). All of the transition state structures exhibit similar AdoMet:Sδ···AdoMet:Cϵ···pEA:N linear geometry (~170 ± 4°) with a reactive methyl species located in the middle between bond breaking and forming (average distance of 2.22 ± 0.02 and 2.23 ± 0.05 Å, respectively). The observed fluctuation of the methyl transfer energy barriers (Table 4) is related to the closeness of the reactant conformations to the in-line transition state features. For instance, the higher barrier of the M3 model (14.8 kcal/mol) is due to the longer bond length of AdoMet:Cϵ···pEA:N and larger deviation of the AdoMet:Sδ···AdoMet:Cϵ···pEA:N angle from the linear attacking angle. We should underline that, for each frame, we also attempted QM/MM calculations driving deprotonation of NH_3^+-pEA through the Tyr-19–His-132 dyad. These simulations, however, resulted again in highly endothermic and monotonically increasing energy profiles analogous to the one shown in Fig. 2*A*.

Biochemical Analysis of PfPMT Asp-128 Site-directed Mutants—To probe the potential role of Asp-128 in the reactions catalyzed by PfPMT, four site-directed mutants (D128A, D128E, D128Q, and D128N) were generated for biochemical analysis. Each mutant was expressed in *E. coli* and was purified by nickel-affinity and size-exclusion chromatographies. All the mutants were isolated as soluble monomeric proteins with expression yields comparable with wild-type PfPMT. The methylation activity of wild-type PfPMT and the four Asp-128 mutants were compared using AdoMet and either pEA (first methylation reaction) or pDME (third methylation reaction) as substrates (Fig. 6). Using pEA and AdoMet as substrates, the D128A, D128E, D128Q, and D128N mutants displayed 1.5, 9.3, 0.6, and 0.2% of wild-type methylation activity, respectively. In contrast, using pDME and AdoMet as substrates, three of the Asp-128 mutants were either comparable (D128A and D128Q) to or had slightly higher (1.8-fold; D128E) specific activities than PfPMT. The D128N mutant showed a 4-fold reduction in specific activity with pDME and AdoMet as substrates.

Determination of steady-state kinetic parameters for the D128A and D128N mutants using either pEA or pDME showed a similar difference between these substrates (Table 5). Both mutations increased the K_m values and decreased the turnover rates with pEA compared with wild-type enzyme. The combination of effects reduced the catalytic efficiencies (k_{cat}/K_m) of the D128A and D128N mutants with pEA by 12,400- and 135,000-fold, respectively. In contrast, the k_{cat}/K_m values for pDME with the D128A and D128N mutants were reduced by 18- and 36-fold, respectively. These results demonstrate that Asp-128 plays a critical role in the methylation of pEA and has a greatly diminished but still significant role in the methylation of pDME.

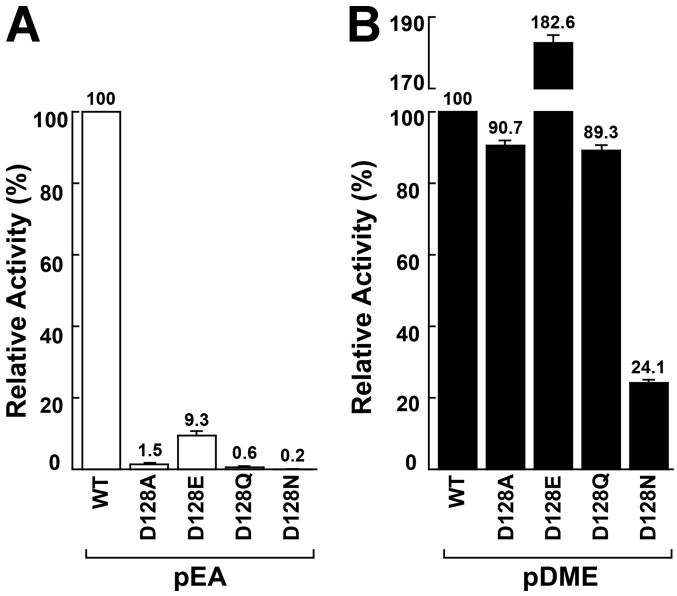

FIGURE 6. **Comparison of wild-type and Asp-128 mutant PfPMT activities.** Relative specific activities are plotted *versus* wild-type PfPMT using pEA (*A*) and pDME (*B*). Standard assay conditions were used. Average values ($n = 3$) with S.E. of less than 5% are shown.

TABLE 5

Steady-state kinetic comparison of wild type (WT), D128A, and D128N PfPMT

Reactions were performed as described under "Experimental Procedures." All parameters are expressed as an average ± S.E. for $n = 3$.

Protein	Substrate	k_{cat}	K_m	k_{cat}/K_m
		min^{-1}	μM	$_M^{-1}s^{-1}$
PfPMT-WT	pEA	109 ± 2	54 ± 4	33,640
PfPMT-WT	pDME	185 ± 14	181 ± 45	17,035
PfPMT-D128A	pEA	1.3 ± 0.1	7,990 ± 1,650	2.71
PfPMT-D128A	pDME	89 ± 23	786 ± 63	1,887
PfPMT-D128N	pEA	0.32 ± 0.07	21,170 ± 7,410	0.25
PfPMT-D128N	pDME	22 ± 1	773 ± 90	474

Ligand Binding and X-ray Crystal Structure of the D128A PfPMT Mutant—To further examine the effect of substitutions of Asp-128, the PfPMT D128A mutant was chosen for additional study by ITC and x-ray crystallography. Given the loss of specific activity observed with this mutant, ITC was used to quantify ligand binding to the enzyme (Fig. 7; Table 6). This analysis shows that mutation of Asp-128 to an alanine does not significantly change the binding affinity for AdoHcy, although the enthalpic and entropic contributions to AdoHcy binding differ compared with wild-type PfPMT (Table 6). For binding of pCho to the D128A mutant, there was insufficient heat signature to accurately determine a K_d value by ITC.

The structural effects of the Asp-128 to alanine mutation were determined by solving the three-dimensional structure of the PfPMT D128A mutant by molecular replacement. The x-ray crystal structures of the mutant protein in complex with AdoHcy and either pCho or pEA were solved to 1.59 and 2.60 Å resolution, respectively (Table 2). The overall structures of the PfPMT-D128A·AdoHcy·pCho and PfPMT-D128A·AdoHcy·pEA complexes were superimposable on the wild-type structure with 0.17 and 0.18 Å r.m.s.d., respectively, for 257 Cα atoms (Fig. 8*A*). As described previously (18, 19), the AdoHcy-binding site of PfPMT is situated along the N-terminal

TABLE 6

ITC analysis of AdoHcy and pCho binding to wild type (WT) and D128A PfPMT

Titrations were performed at 20 °C and data fit to a single-site binding model. ND = not detected.

Protein	Ligand	K_d	ΔG	ΔH	$-T\Delta S$
		μM	*kcal/mol*	*kcal/mol*	*kcal/mol*
WT	AdoHcy	7.6 ± 0.4	−6.8 ± 0.4	−12.1 ± 0.2	5.2
D128A	AdoHcy	5.4 ± 0.1	−7.1 ± 0.1	−18.7 ± 0.0	11.6
WT	pCho	20.0 ± 0.3	−6.3 ± 0.1	−20.1 ± 0.1	13.8
D128A	pCho	ND	ND	ND	ND

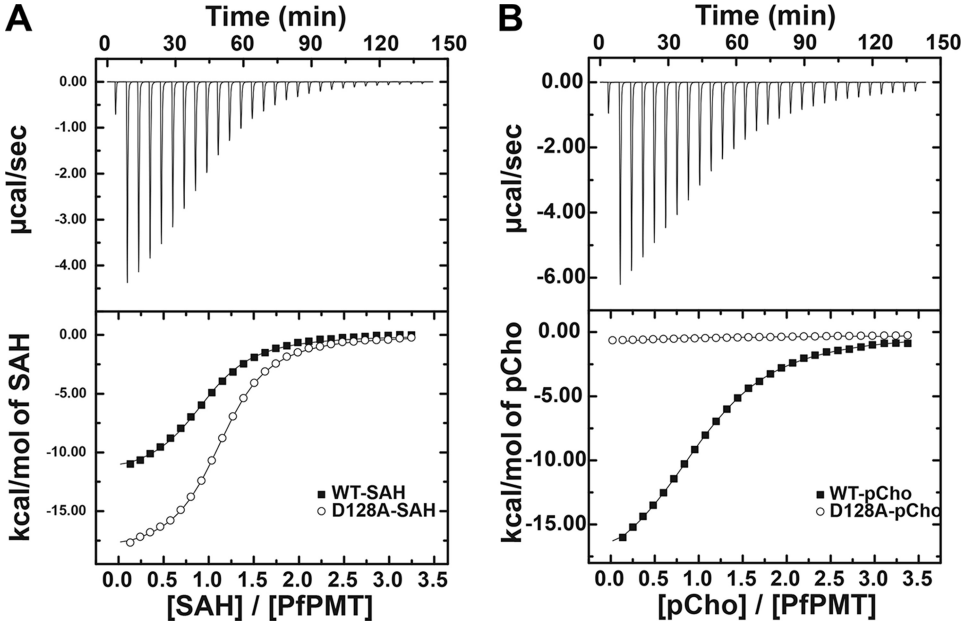

FIGURE 7. **ITC analysis of ligand binding to wild-type and D128A PfPMT.** *A,* titration of wild-type PfPMT (*solid squares*) and PfPMT-D128A mutant (*open circles*) with AdoHcy (*SAH*). The *top panel* shows data plotted as heat signal (μcal s^{-1}) *versus* time (min). The experiment consisted of 28 injections of 10 μl of AdoHcy (1250 μM) into a solution containing PfPMT (80 μM) at 20 °C. The *bottom panel* shows the integrated heat response per injection from *A* plotted as normalized heat per mol of injectant. The *solid line* represents the fit to the data. *B,* titration of wild-type PfPMT (*solid squares,* 80 μM) and PfPMT-D128A mutant (*open circles,* 80 μM) with pCho (1,300 μM). *Top* and *bottom panels* are as in *A*.

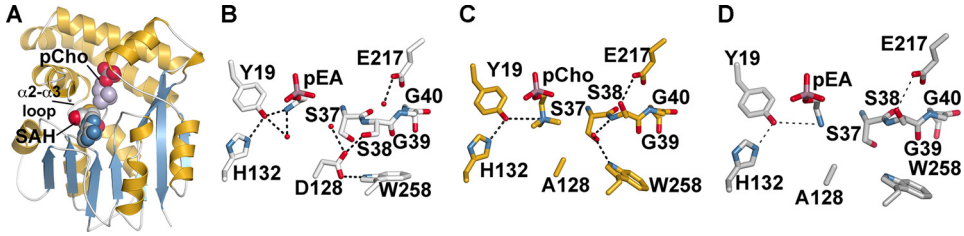

FIGURE 8. **Structural comparison of the wild-type and D128A PfPMT active sites.** *A,* overall structure of the PfPMT-D128A·AdoHcy·pCho complex. AdoHcy and pCho are shown as space-filling models. The position of the α2-α3 loop, which includes Ser-37–Gly-40, is indicated. *B,* active site view of the PfPMT·AdoHcy·pEA complex (18). AdoHcy is not shown for clarity. Key water molecules are shown as *red spheres*. Hydrogen bonds are indicated by *dashed lines*. *C,* active site view of the PfPMT-D128A·AdoHcy·pCho complex. AdoHcy is not shown for clarity. Key water molecules are shown as *red spheres*. Hydrogen bonds are indicated by *dashed lines*. *D,* active site view of the PfPMT-D128A·AdoHcy·pEA complex. AdoHcy is not shown for clarity. Key water molecules are shown as *red spheres*. Hydrogen bonds are indicated by *dashed lines*.

side of the β-sheet forming the core of the protein, and the phosphobase site is capped by an α-helical domain (Fig. 8*A*). No significant structural changes were observed in the AdoHcy/AdoMet-binding site of the D128A mutant *versus* the wild-type enzyme.

Comparison of the previously determined PfPMT structure (Fig. 8*B*) (18) with the crystal structures of PfPMT-D128A·AdoHcy·pCho (Fig. 8*C*) and PfPMT-D128A·AdoHcy·pEA (Fig. 8*D*) complexes shows that mutation of Asp-128 to an alanine disrupts a hydrogen bond network observed in the wild-type enzyme. This disruption leads to structural changes in the active site, especially in the positioning of residues in the α2-α3 loop (Ser-37–Gly-40). Within the wild-type PfPMT active site (18) (Fig. 8*B*), the carboxylate side chain of Asp-128 is oriented away from bound pEA and forms hydrogen bond interactions with Trp-258 (2.9 Å), Ser-38 (2.7 Å), and a water molecule (2.8 Å). In the D128A mutant, removal of the Asp-128 carboxylate group leads to Trp-258 rotating 21° to form a new hydrogen bond between the indole nitrogen and a water molecule (3.3 Å), which is also bound by the backbone nitrogen of Ser-38 (3.1 Å). The loss of the Asp-128–Ser-38 interaction shifts the peptide backbone of Ser-37 and Ser-38 1.5–1.6 Å away from Ala-128. Concomitant rotation of the side chain hydroxyl of Ser-38 moves this moiety 3.6 Å from the position observed in the wild-type enzyme and leads to formation of a new hydrogen bond with the carboxylate of Glu-217 (2.9 Å). This displaces a water molecule that was bound by the glutamate side chain in the wild-type active site. The PfPMT-D128A·AdoHcy·pEA complex shows similar structural rearrangements in the active site (Fig. 8*D*).

Although Asp-128 does not form any direct contacts with phosphobase substrates, the observed structural changes alter positioning of the reactive amine group. Substitution of Asp-128 with an alanine and the resulting shift of the α2-α3 loop provides additional space in the active site that allows more conformational flexibility for the amine group of a bound phosphobase molecule. For example, the distances between the hydroxyl group of Tyr-19 and the substrate nitrogen in the PfPMT·AdoHcy·pEA (Fig. 8*B*), the PfPMT-D128A·AdoHcy·pCho (Fig. 8*C*), and the PfPMT-D128A·AdoHcy·pEA (Fig. 8*D*) complexes are 2.5, 3.9, and 4.4 Å, respectively.

Effect of the D128A Mutation on Active Site Mobility in MD Simulations—Given the structural changes resulting from mutation of Asp-128 to an alanine, MD simulations were used to examine the consequences of the mutation on active site dynamics. Three different 10-ns trajectories for wild-type and D128A PfPMT were generated. The average binding free energy (ΔG) of NH_3^+-pEA estimated by the MM/GBSA approach (31) suggests weaker affinity to the mutant, with values of −16.8 and −7.3 kcal/mol for wild-type and D128A mutant, respectively. In addition to altering the active site architecture, removal of the carboxylate side chain in the D128A mutant allows for greater mobility of active site residues and diffusion of water molecules from the bulk, as indicated by MD simulations (Fig. 9, *A* and *B*). Analysis of water molecules within 5 Å of the AdoMet:Cϵ atom indicates the presence of 1–2 water molecules in the PfPMT, but 1–4 water molecules for the D128A mutant (Fig. 9*C*). Overall, the increased active site mobility translates into a longer distances between AdoMet and the NH_3 group of pEA (Fig. 9*D*), in agreement with the crystallographic observations, as described above. For both wild-type and D128A, the phosphate group of pEA is comparatively restrained due to multiple interactions with Tyr-27, Tyr-160, Tyr-175, Arg-179, Tyr-181, and Lys-247.

DISCUSSION

Although AdoMet-dependent methylations of macromolecules and metabolites are ubiquitous in biological systems, the enzymes that perform these transformations employ a variety of chemical strategies (1). Most methyltransferases follow a common S_n2 methyl transfer mechanism following proton transfer from the substrate to a catalytic base in either stepwise or concerted mechanisms (2, 36–41). The identification of a family of PMT from plants, nematodes, and the malaria parasite *P. falciparum* provides an opportunity to explore the structural and chemical evolution of diverse methyltransferase active site architectures that catalyze the steps of the phosphobase methylation pathways in these organisms (Fig. 1, *top*) (4–12).

Using PfPMT, we examined the methylation of pEA using a combined computation, biochemical, and structural approach. In pEA methylation catalyzed by PfPMT, the substrate must be deprotonated for catalysis to occur. Based on a series of x-ray crystal structures, ligand binding studies, and the analysis of site-directed mutants of PfPMT, a reaction mechanism involving the Tyr-19–His-132 dyad was proposed (Fig. 1, *bottom*) (18). To examine the energetics of this mechanism, QM/MM calculations were used to obtain the energy profile for deprotonation and methylation of pEA. Overall, the simulations reveal features in common with other methyltransferase reactions

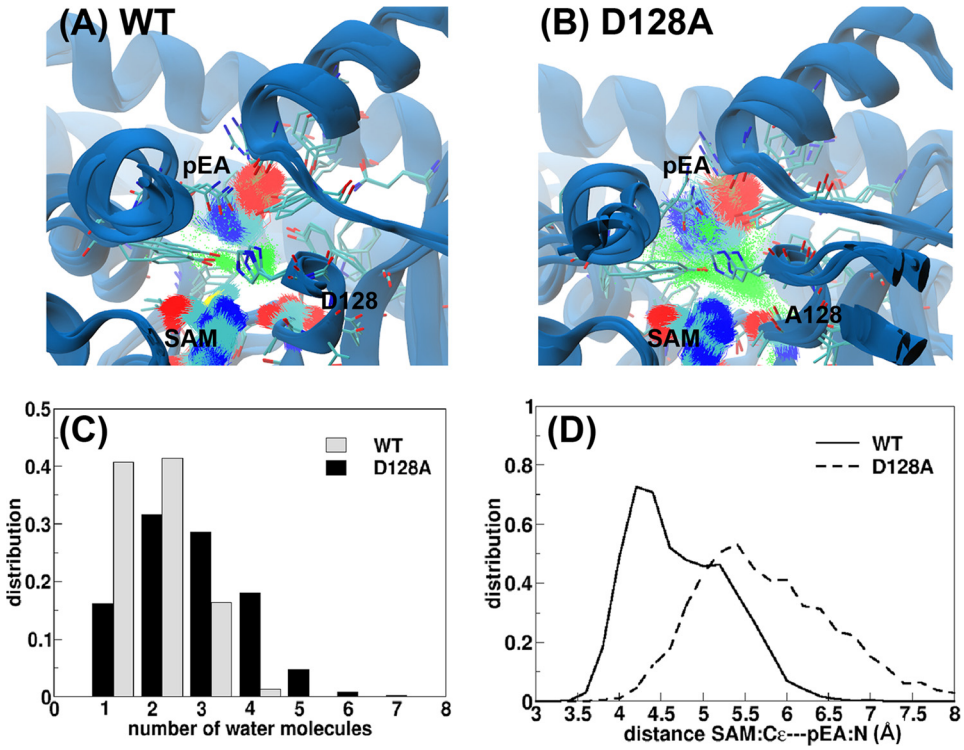

FIGURE 9. **Average structural analyses comparing the wild-type and D128A PfPMT over three MD trajectories.** *A* and *B* show the superimposition of MD snapshots showing the distribution of water positions (*green dot*) and increase in flexibility in the active sites of wild-type (*A*) and D128A (*B*). *C,* histogram plot of the number of water molecules found within 5 Å of the Cϵ of AdoMet. *D,* distribution of the methyl transfer distance (AdoMet:Cϵ···pEA:N) in wild-type and D128A. *SAM* is AdoMet.

and provide new molecular insight on the first step of the phosphobase methylation pathway.

The simulations clearly indicate an unfavorable energetic reaction coordinate for the proposed catalytic role of His-132 as a general base to activate Tyr-19 in deprotonating a charged (*i.e.* NH_3^+-pEA) substrate (Fig. 2*A*). Interestingly, during the QM/MM simulation, rotation of the amine group of pEA toward a water molecule bound to Asp-128 was observed and suggested an alternative reaction mechanism (Fig. 2*B*). This rotation aids in formation of a hydrogen bond network and correlates with the relatively high value of *B*-factor of this moiety in x-ray crystal structure (18), which supports the mobility of the substrate amine observed in the simulation. The QM/MM reaction coordinate profiles suggest that the methylation of pEA catalyzed by PfPMT proceeds through the stepwise mechanism starting with the proton transfer step from NH_3^+-pEA to Asp-128 through a water bridge. This is followed by the methyl transfer from AdoMet to NH_2-pEA to form the product. The overall stepwise mechanism is an exothermic process with methyl transfer as the rate-limiting step; the presence of high barriers excludes a concerted methyl transfer/proton transfer pathway.

For this alternative mechanism in PfPMT, the core features of the methyltransferase reaction are consistent with other computational studies. The QM/MM calculations on multiple starting configurations of the PfPMT active site address the potential dynamical nature of the enzyme and indicates that they do not alter the mechanism (42). Our results indeed support the hypothesis from Hu and Zhang (39) that an indicator for the reactivity for such a methyl transfer reaction is a combination of the nucleophilic attack bond length (*d)* and angle (θ) (Table 4). In addition, the calculated average energy barrier of 9.7 ± 3.2 kcal/mol obtained from the M06/6–31G(d,p)/OPLS calculation for the methylation of pEA is in agreement with the activation barrier of 9.6 kcal/mol estimated from the experimental value of k_{cat} = 109 min^{-1} (18) and the simple transition state theory: $k(T) = (k_b T/h)\exp(-\Delta G/RT)$. To further validate this mechanism, a combination of site-directed mutagenesis, biochemical assays, and protein crystallography were performed.

Biochemical analysis of the PfPMT D128A, D128N, D128Q, and D128E site-directed mutants confirms an important functional role for Asp-128 in the methylation of pEA; however, the specific activities of the mutants remain comparable with wild-type enzyme for the conversion of pDME to pCho (Fig. 6). Steady-state kinetic analysis of the D128A and D128N mutants indicate that either removal of the carboxylic acid group or substitution with an amide group reduces k_{cat} with pEA by 100–300-fold (Table 5). In addition, these changes significantly increase the K_m values for pEA (Table 5). Consistent with the specific activity measurements, the D128A and D128N mutants displayed more modest changes in kinetic parameters for pDME. This suggests a specific role for Asp-128 during the first step of the phosphobase methylation pathway catalyzed by PfPMT.

Ligand binding analysis of the PfPMT D128A mutant using ITC indicates that this mutation does not alter AdoHcy binding (Fig. 7*A*; Table 6), as expected from this residue's position in the three-dimensional structure. In comparison, the D128A substitution alters pEA and pCho binding, even though the aspartate makes no direct contacts with phosphobase substrates. Although the bind-

ing constant for pCho could not be accurately determined because of a lack of heat signature (Fig. 7*B*; Table 6), use of saturating concentrations of pEA and pCho during protein crystallization allowed for determination of the x-ray crystal structure of the PfPMT D128A mutant in the presence of each ligand (Fig. 8; Table 6). The initial inspection of the crystals confirms that mutating Asp-128 does not change the overall positioning of AdoHcy, pEA, and pCho in the active site. The network of interactions centered on Asp-128 in the wild-type enzyme, however, is disrupted in the mutant enzyme, inducing a larger mobility in pEA's amine group. Those changes, reducing the probability of reactive conformations with reasonable distances between the methyl donor and acceptor (43), are nicely reproduced by MD simulations of the D128A mutant (Fig. 9).

Although the residue corresponding to Asp-128 of PfPMT is invariant across other PMT from plants and nematodes (6), the structural context of this aspartate differs in these enzymes. The x-ray crystal structures of PMT1 and PMT2 from the nematodes *C. elegans* and *Haemonchus contortus* reveal two distinct active site architectures (11) as follows: one for the methylation of pEA (PMT1) and another for the methylations of pMME and pDME (PMT2). Intriguingly, PMT2 from *C. elegans* and *H. contortus* do not use pEA as a substrate, even though these enzymes share an active site architecture nearly identical to PfPMT (11, 18). To understand how the PfPMT catalyzes the methylation of pEA, sequence and structural comparisons identified a difference between Ser-38 of PfPMT and a proline at the same position in the nematode PMT2 enzymes (11). These comparisons show that the interface of the AdoMet/AdoHcy and phosphobase-binding site of the nematode PMT2 is more constricted compared with PfPMT. This constriction in the nematode enzymes prevents water molecules from binding in the active site near the phosphobase amine. Because the extra space in PfPMT allows water molecules to enter the active site, it was previously suggested that the water network helps to orient the amine group of pEA for catalysis in PfPMT (11). A point mutation in PfPMT (*i.e.* S38P) eliminated activity of the enzyme with pEA but retained wild-type activity with pDME (11). That result mimics the effects of the D128A, D128Q, D128N, and D128E mutants in PfPMT (Fig. 6). Moreover, mutation of Asp-128 to an alanine in PfPMT shifts Ser-37–Gly-40 of the α2-α3 loop to a position similar to that of the same loop in the active site of the PMT2 from *C. elegans* and *H. contortus* (11). Additional MD simulations for an S38P mutant clearly indicate the disruption of the hydrogen bond network (and the dehydration) between pEA and Asp-128 (Fig. 10). These results highlight the subtle changes in the PfPMT active site required for use of pEA as a substrate.

In conclusion, we suggest a new catalytic role for Asp-128 in the active site of PfPMT. The first contribution of Asp-128 is that of a general base to activate a water molecule that aids in deprotonation of pEA, as suggested by the QM/MM calculations described here. In contrast to the active sites of the nematode PMT2 (11), the PfPMT active site readily accommodates water molecules that form a hydrogen bond network involving Asp-128. Importantly, this structural difference is linked to the interaction between Asp-128 and Ser-38, which shifts the α2-α3 loop to allow for the water network in PfPMT. These structural changes are important for the evolution of an alternate reaction path for pEA methylation by PfPMT.

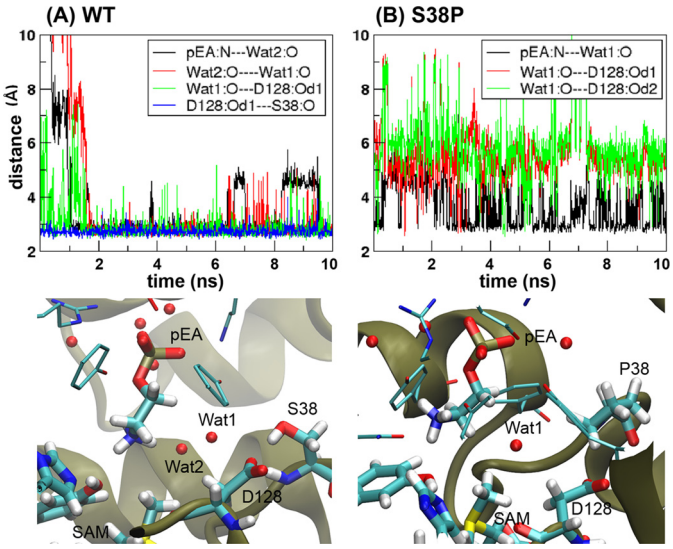

FIGURE 10. **Comparison of wild-type and S38P PfPMT active sites in MD simulations.** Plot of distances between pEA, water-bridged molecules, Asp-128, and Ser-38 (or Pro-38) from 10-ns MD simulations of wild-type (*A*) and S38P mutant PfPMT (*B*). A representative snapshot is also shown.

REFERENCES

1. Liscombe, D. K., Louie, G. V., and Noel, J. P. (2012) Architectures, mechanisms, and molecular evolution of natural product methyltransferases. *Nat. Prod. Rep.* **29,** 1238–1250
2. Smith, B. C., and Denu, J. M. (2009) Chemical mechanisms of histone lysine and arginine modifications. *Biochim. Biophys. Acta* **1789,** 45–57
3. Schapira, M. (2011) Structural chemistry of human SET domain protein methyltransferases. *Curr. Chem. Genomics* **5,** 85–94
4. McNeil, S. D., Nuccio, M. L., Ziemak, M. J., and Hanson, A. D. (2001) Enhanced synthesis of choline and glycine betaine in transgenic tobacco plants that overexpress phosphoethanolamine *N*-methyltransferase. *Proc. Natl. Acad. Sci. U.S.A.* **98,** 10001–10005
5. Bobenchik, A. M., Augagneur, Y., Hao, B., Hoch, J. C., and Ben Mamoun, C. (2011) Phosphoethanolamine methyltransferases in phosphocholine biosynthesis: functions and potential for antiparasite therapy. *FEMS Microbiol. Rev.* **35,** 609–619
6. Lee, S. G., and Jez, J. M. (2014) Nematode phospholipid metabolism: an example of closing the genome-structure-function circle. *Trends Parasitol.* **30,** 241–250
7. Nuccio, M. L., Ziemak, M. J., Henry, S. A., Weretilnyk, E. A., and Hanson, A. D. (2000) cDNA cloning of phosphoethanolamine *N*-methyltransferase from spinach by complementation in *Schizosaccharomyces pombe* and characterization of the recombinant enzyme. *J. Biol. Chem.* **275,** 14095–14101
8. Palavalli, L. H., Brendza, K. M., Haakenson, W., Cahoon, R. E., McLaird, M., Hicks, L. M., McCarter, J. P., Williams, D. J., Hresko, M. C., and Jez, J. M. (2006) Defining the role of phosphomethylethanolamine *N*-methyltransferase from *Caenorhabditis elegans* in phosphocholine biosynthesis by biochemical and kinetic analysis. *Biochemistry* **45,** 6056–6065
9. Brendza, K. M., Haakenson, W., Cahoon, R. E., Hicks, L. M., Palavalli, L. H., Chiapelli, B. J., McLaird, M., McCarter, J. P., Williams, D. J., Hresko, M. C., and Jez, J. M. (2007) Phosphoethanolamine *N*-methyltransferase (PMT-1) catalyzes the first reaction of a new pathway for phosphocholine biosynthesis in *Caenorhabditis elegans*. *Biochem. J.* **404,** 439–448
10. Lee, S. G., Haakenson, W., McCarter, J. P., Williams, D. J., Hresko, M. C., and Jez, J. M. (2011) Thermodynamic evaluation of ligand binding in the plant-like phosphoethanolamine methyltransferases of the parasitic nematode *Haemonchus contortus*. *J. Biol. Chem.* **286,** 38060–38068
11. Lee, S. G., and Jez, J. M. (2013) Evolution of structure and mechanistic divergence in di-domain methyltransferases from nematode phospho-

choline biosynthesis. *Structure* **21,** 1778–1787
12. Pessi, G., Kociubinski, G., and Mamoun, C. B. (2004) A pathway for phosphatidylcholine biosynthesis in *Plasmodium falciparum* involving phosphoethanolamine methylation. *Proc. Natl. Acad. Sci. U.S.A.* **101,** 6206–6211
13. Witola, W. H., El Bissati, K., Pessi, G., Xie, C., Roepe, P. D., and Mamoun, C. B. (2008) Disruption of the *Plasmodium falciparum* PfPMT gene results in a complete loss of phosphatidylcholine biosynthesis via the serine-decarboxylase-phosphoethanolamine-methyltransferase pathway and severe growth and survival defects. *J. Biol. Chem.* **283,** 27636–27643
14. Bobenchik, A. M., Witola, W. H., Augagneur, Y., Nic Lochlainn, L., Garg, A., Pachikara, N., Choi, J. Y., Zhao, Y. O., Usmani-Brown, S., Lee, A., Adjalley, S. H., Samanta, S., Fidock, D. A., Voelker, D. R., Fikrig, E., and Ben Mamoun, C. (2013) *Plasmodium falciparum* phosphoethanolamine methyltransferase is essential for malaria transmission. *Proc. Natl. Acad. Sci. U.S.A.* **110,** 18262–18267
15. Calas, M., Ancelin, M. L., Cordina, G., Portefaix, P., Piquet, G., Vidal-Sailhan, V., and Vial, H. (2000) Antimalarial activity of compounds interfering with *Plasmodium falciparum* phospholipid metabolism: comparison between mono- and bisquaternary ammonium salts. *J. Med. Chem.* **43,** 505–516
16. Wengelnik, K., Vidal, V., Ancelin, M. L., Cathiard, A. M., Morgat, J. L., Kocken, C. H., Calas, M., Herrera, S., Thomas, A. W., and Vial, H. J. (2002) A class of potent antimalarials and their specific accumulation in infected erythrocytes. *Science* **295,** 1311–1314
17. Hunter, W. N. (2009) Structure-based ligand design and the promise held for antiprotozoan drug discovery. *J. Biol. Chem.* **284,** 11749–11753
18. Lee, S. G., Kim, Y., Alpert, T. D., Nagata, A., and Jez, J. M. (2012) Structure and reaction mechanism of phosphoethanolamine methyltransferase from the malaria parasite *Plasmodium falciparum*–an anti-parasitic drug target. *J. Biol. Chem.* **287,** 1426–1434
19. Lee, S. G., Alpert, T. D., and Jez, J. M. (2012) Crystal structure of phosphoethanolamine methyltransferase from *Plasmodium falciparum* in complex with amodiaquine. *Bioorg. Med. Chem. Lett.* **22,** 4990–4993
20. Sastry, G. M., Adzhigirey, M., Day, T., Annabhimoju, R., and Sherman, W. (2013) Protein and ligand preparation: parameters, protocols, and influence on virtual screening enrichments. *J. Comput. Aided Mol. Des.* **27,** 221–234
21. Sondergaard, C. R., Olsson, M. H., Rostkowski, M., and Jensen, J. H. (2011) Improved treatment of ligands and coupling effects in empirical calculation and rationalization of pK_a values. *J. Chem. Theory Comp.* **7,** 2284–2295
22. Zhang, X., and Bruice, T. C. (2008) Enzymatic mechanism and product specificity of SET-domain protein lysine methyltransferase. *Proc. Natl. Acad. Sci. U.S.A.* **105,** 5728–5732
23. Zhao, Y., and Truhlar, D. G. (2008) The M06 suite of density functions for main group thermochemistry, thermochemical kinetics, noncovalent interactions, excited states, and transition elements: two new functionals and systematic testing of four M06-class functionals and 12 other functionals. *Theor. Chem. Acc.* **120,** 215–241
24. Jorgensen, W. L., Maxwell, D. S., and Tirado-Rives, J. (1996) Development and testing of the OPLS all-atom force field on conformational energetics and properties of organic liquids. *J. Am. Chem. Soc.* **118,** 11225–11236
25. Duan, Y., Wu, C., Chowdhury, S., Lee, M. C., Xiong, G., Zhang, W., Yang, R., Cieplak, P., Luo, R., Lee, T., Caldwell, J., Wang, J., and Kollman, P. (2003) A point-charge force field for molecular mechanics simulations of proteins based on condensed-phase quantum mechanical calculations. *J. Comput. Chem.* **24,** 1999–2012
26. Wang, J., Wolf, R. M., Caldwell, J. W., Kollman, P. A., and Case, D. A. (2004) Development and testing of a general amber force field. *J. Comput. Chem.* **25,** 1157–1174
27. Bayly, C. I., Cieplak, P., Cornell, W., and Kollman, P. A. (1993) A well-behaved electrostatic potential based method using charge restraints for deriving atomic charges: the RESP model. *J. Phys. Chem.* **97,** 10269–10280
28. Darden, T., York, D., and Pedersen, L. G. (1993) Particle mesh Ewald: an *N*log(*N*) method for Ewald sums in large systems. *J. Chem. Phys.* **98,** 10089–10092
29. Ryckaert, J. P., Ciccotti, G., and Berendsen, H. J. C. (1977) Numerical integration of the cartesian equations of motion of a system with constraints: molecular dynamics of *n*-alkanes. *J. Comp. Phys.* **23,** 327–341
30. Roe, D. R., and Cheatham, T. E. (2013) PTRAJ and CPPTRAJ: software for processing and analysis of molecular dynamics trajectory data. *J. Chem. Theory Comp.* **9,** 3084–3095
31. Kollman, P. A., Massova, I., Reyes, C., Kuhn, B., Huo, S., Chong, L., Lee, M., Lee, T., Duan, Y., Wang, W., Donini, O., Cieplak, P., Srinivasan, J., Case, D. A., and Cheatham, T. E. (2000) Calculating structures and free energies of complex molecules: combining molecular mechanics and continuum models. *Acc. Chem. Res.* **33,** 889–997
32. Minor, W., Cymborowski, M., Otwinowski, Z., and Chruszcz, M. (2006) HKL-3000: the integration of data reduction and structure solution- from diffraction images to an initial model in minutes. *Acta Crystallogr. D Biol. Crystallogr.* **62,** 859–866
33. McCoy, A. J., Grosse-Kunstleve, R. W., Adams, P. D., Winn, M. D., Storoni, L. C., and Read, R. J. (2007) Phaser crystallographic software. *J. Appl. Crystallogr.* **40,** 658–674
34. Emsley, P., and Cowtan, K. (2004) Coot: model-building tools for molecular graphics. *Acta Crystallogr. D Biol. Crystallogr.* **60,** 2126–2132
35. Adams, P. D., Afonine, P. V., Bunkóczi, G., Chen, V. B., Davis, I. W., Echols, N., Headd, J. J., Hung, L. W., Kapral, G. J., Grosse-Kunstleve, R. W., McCoy, A. J., Moriarty, N. W., Oeffner, R., Read, R. J., Richardson, D. C., Richardson, J. S., Terwilliger, T. C., and Zwart, P. H. (2010) PHENIX: a comprehensive Python-based system for macromolecular structure solution. *Acta Crystallogr. D Biol. Crystallogr.* **66,** 213–221
36. Cheng, X., Collins, R. E., and Zhang, X. (2005) Structural and sequence motifs of protein (histone) methylation enzymes. *Annu. Rev. Biophys. Biomol. Struct.* **34,** 267–294
37. Velichkova, P., and Himo, F. (2005) Methyl transfer in glycine *N*-methyltransferase: a theoretical study. *J. Phys. Chem. B* **109,** 8216–8219
38. Velichkova, P., and Himo, F. (2006) Theoretical study of the methyl transfer in guanidinoacetate methyltransferase. *J. Phys. Chem. B* **110,** 16–19
39. Hu, P., and Zhang, Y. (2006) Catalytic mechanism and product specificity of the histone lysine methyltransferase SET7/9: an *ab initio* QM/MM-FE study with multiple initial structures. *J. Am. Chem. Soc.* **128,** 1272–1278
40. Zhang, X., and Bruice, T. C. (2006) Reaction mechanism of guanidinoacetate methyltransferase, concerted or step-wise. *Proc. Natl. Acad. Sci. U.S.A.* **103,** 16141–16146
41. Schmidt, T., Schwede, T., and Meuwly, M. (2014) Computational analysis of methyl transfer reactions in dengue virus methyltransferase. *J. Phys. Chem. B* **118,** 5882–5890
42. Zhang, Y., Kua, J., and McCammon, J. A. (2003) Influence of structural fluctuation on enzyme reaction energy barriers in combined quantum mechanical/molecular mechanical studies. *J. Phys. Chem. B.* **107,** 4459–4463
43. Hur, S., and Bruice, T. C. (2003) The near attack conformation approach to the study of the chorismate to prephenate reaction. *Proc. Natl. Acad. Sci. U.S.A.* **100,** 12015–12020